PERFORMANCE EVALUATION OF A BOUNDARY LAYER DIVERTER FOR SUPERSONIC PROPULSION SYSTEM

H. Miki*, Y. Watanabe, M. Kameda***
***Tokyo Univ. of Agriculture and Technology, **JAXA**
50012833010@st.tuat.ac.jp; wata@chofu.jaxa.jp; kame@cc.tuat.ac.jp

Keywords: *propulsion/airframe integration, supersonic air-inlet, CFD, wind tunnel test*

Abstract

A parametric study on configurations of a diverter using CFD simulation was conducted to examine those effects on the performance of diverter. It is found that, in design process of diverter, firstly, the width of diverter should be set to minimum value, then, the apex angle and the height should be optimized.

Additionally, the inlet ramp configuration which prevents the boundary-layer ingestion into the inlet was also examined for the purpose of achieving drag reduction by decreasing diverter height. Wind tunnel test was conducted to validate results of CFD analysis. It was found that the cone ramp is one of the effective measures to reduce the boundary-layer flows into a subsonic diffuser.

1 Introduction

Research activity on next generation supersonic transport (SST) increases because of the retirement of Concorde SST [1]. Compromise design of airframe and propulsion system must be needed to achieve good aerodynamic performance in SST.

Supersonic air-inlet is one of the important devices of propulsion system for SST, which decelerates the supersonic flow to subsonic region using several shock-waves and supply adequate air mass flow to engine through a subsonic diffuser (see Fig.1). Removing boundary-layer on the airframe surface at some stage from the inlet is important to improve performance of propulsion system [2]. The diverter is one of the means to do this, which implies that the inlet stands off from a particular surface, allowing the boundary-layer on that surface to escape down the intermediate channel.

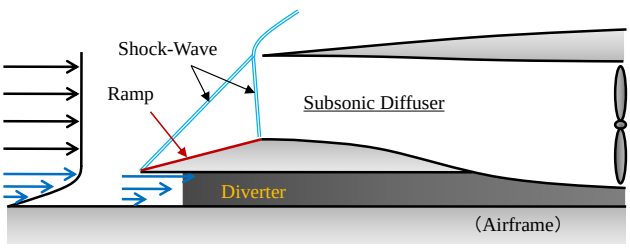

Fig.1 Supersonic air-inlet and diverter

The higher diverter compared with boundary-layer thickness can reduce total-pressure loss of inlet [3]. However, it increases aerodynamic drag of airframe [4], which should be smaller than the improvement in engine net thrust. The diverter is an interface between propulsion system and airframe, so that, its performance should be evaluated mutually in terms of both performances.

In this study, the performance of diverter was set in terms of propulsion system and airframe. A parametric study on configurations of a diverter using CFD simulation was conducted to examine those effects on the performance of diverter. The guideline to design the diverter which provides better performance was discussed by rounding up the results of CFD analysis.

Additionally, in order to achieve the reduction of drag caused from propulsion/airframe integration design, it is preferable to mount the inlet on the airframe without diverter. In that case, the inlet has to tolerate the thick boundary-layer ingestion, and a new design technique of inlet is needed.

Ramp is a composition element of inlet, it causes several shock-waves to compress (to decrease) the supersonic flow in the upstream of subsonic diffuser (Fig.1). It is thought that decreasing the boundary-layer flows into a subsonic diffuser from a ramp is one of the approaches to maintain the performance of diverterless supersonic inlet.

In this study, CFD analysis was employed to examine the ramp configuration which decreases the thickness of boundary-layer flows into a subsonic diffuser and compresses the air-flow sufficiently. Furthermore, wind tunnel test was performed to validate the result of CFD analysis.

2 Performance Evaluation of Diverter

2.1 Diverter Model

In order to examine changes of flow field due to diverter easily, a simple diverter model without air-inlet was used in this study. Figure 2 shows the schematic of the diverter model. It consists of a zero thickness flat plate instead of air-inlet, a diverter and a flat board as airframe surface. The diverter has a planar shape like a prow which is designed using Cubic Bezier curve.

Geometry parameters of diverter model are apex angle (θ), diverter height (h), length ratio (L/w) and width ratio (w/w_{FP}). In this study, the width and the length of flat plate are fixed values, because geometries of air-inlet or engine nacelle can't be modified in the design process of diverter.

2.2 CFD Analysis

Figure 3 shows a computational grid which was generated for CFD analysis around the diverter model. Half of the diverter was used as the computational region for saving grid points. The total grid point number was approximately 2.5 million. The computational code owned by Japan Aerospace Exploration Agency, JAXA, was used for numerical calculation, in which the basic equations are 3D-compressive Navier-Stokes equations with the k-ε model as a turbulence model [5].

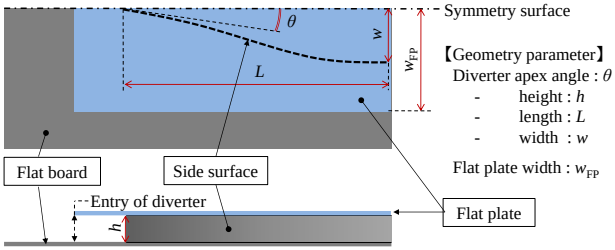

Fig.2 Diverter model

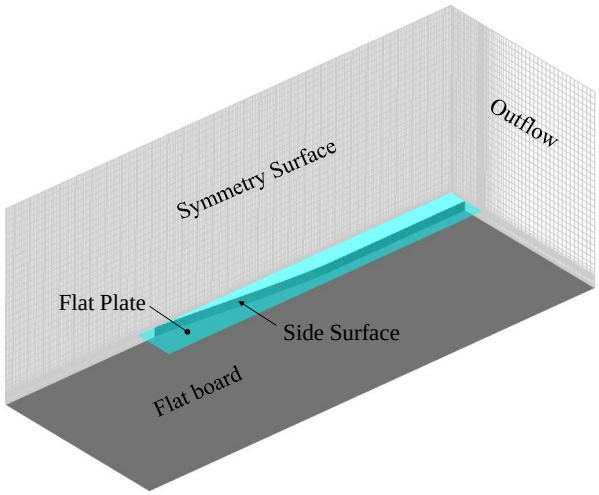

Fig.3 Computational grid for diverter flow

The numerical calculation was carried out at free stream Mach number of 1.3. The Reynolds number based on the flat plate width (w_{FP}) was 5×10^5. Additionally the boundary-layer thickness is characterized using $\delta_{99\%}$, which is defined as the physical height of boundary-layer at 99% of the free stream total-pressure. In order to examine the effect of diverter height (h) to the diverter performance, numerical calculations was conducted under the several condition of non-dimensional boundary-layer heights, $h/\delta_{99\%}$.

2.3 Aerodynamic Performance of Diverter

The diverter has to remove a boundary-layer for maintaining inlet performances, and should be designed to that it doesn't greatly decrease aerodynamic performance of airframe. Therefore, the performance of diverter was evaluated in terms of a removing boundary-layer on the airframe surface and its aerodynamic drag.

The evaluation index of removing boundary-layer was displacement thickness (δ^*) at the entry of diverter (see Fig.2). The smaller δ^* implies that the fewer amount of boundary-layer

would be ingested into an inlet. Specifically, the ratio of displacement thickness and diverter height, h/δ^*, was averaged in the direction of flat plate width, and it was used for evaluation.

The aerodynamic drag of diverter was evaluated by drag coefficient (C_D) based on the product of the flat plate width and the boundary-layer thickness, $w_{FB} \times \delta_{99\%}$.

2.4 Design Guideline of Diverter

The restriction of diverter design which is imposed by demands of airframe and propulsion system will be considered below.

The width of inlet ramp, which corresponds to the width of flat plate (w_{FP}) in this study, can't be modified in the design process of diverter, because it is determined in the inlet design. The maximum value of diverter length (L) depends on the engine-nacelle design. Furthermore, it is thought that the minimum settable value of diverter width (w) exists, because the diverter must lift an inlet from an airframe surface as a part of airframe structure. In order to maintain inlet performances by removing a boundary-layer, the minimum settable value of diverter height (h) also exists. These are principal restrictions of diverter design.

In order to consider the design guideline of diverter, results of CFD analysis are shown in Fig.4, which is the graph with displacement thickness (h/δ^*) on the y-axis and drag coefficient (C_D) on the x-axis. The relationship between the aerodynamic performance and the diverter height is represented as lines connecting data points. For example, the performance of higher diverter shifts to right below of the graph. The region which is closer to left below of the graph implies that low drag and removing much boundary-layer, i.e. diverter is superior in terms of propulsion/airframe integration design.

Because the role of diverter is maintaining inlet performance, its aerodynamic drag should be smaller than the improvement in engine net thrust. As can be seen in Fig.4, drag reduction can be achieved effectively by designing the width ratio (w/w_{FP}) smaller, because the projected area of diverter becomes small relative

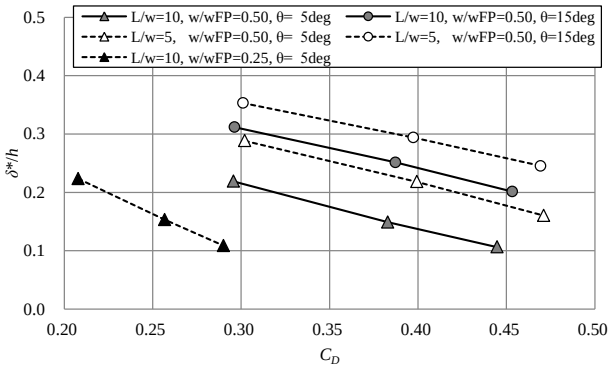

Fig.4 Performance map of diverter

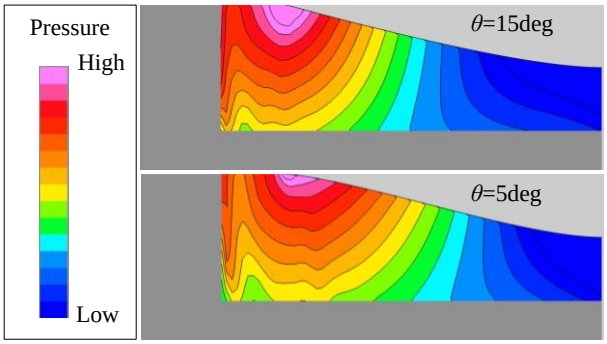

Fig.5 Averaged pressure distribution in channel

to the characteristic area of drag coefficient. In the process of diverter design, it means that the diverter width (w) becomes narrow, because the ramp width (w_{FP}) is fixed value. Furthermore, the narrow diverter makes the length ratio (L/w) large, and improves the performance of removing boundary-layer. This is because that pressure loss which occurs at the inside of channel was decreased. Therefore, it can be said that aerodynamic performances become better by designing the diverter width narrower.

The drag reduction is also achieved by designing the diverter apex angle (θ) smaller. Because the side surface of diverter behaves as the expansive surface when the apex angle is large, so that the pressure drag caused at there is decreased relative to the diverter with the small apex angle. Figure 5 shows the averaged pressure distribution in the channel, and it can be seen that the area of lower pressure region was more widespread when the apex was larger. On the other hand, performance of removing boundary-layer becomes worse with increase of apex angle. Thus it can be said that the effect of apex angle exhibits trade-off in aerodynamic performance of diverter as is the case in the diverter height.

The design guideline of diverter which based on the outcomes of this study will be summarized as below. In the design process of diverter, firstly, the width of diverter should be set to minimum value, then, the apex angle and the height should be optimized.

3 Performance Evaluation of Ramp

3.1 Ramp Model

For the purpose of examining boundary-layer flow around a ramp for diverterless supersonic inlet, a simple ramp model without subsonic diffuser was used in this study. Figure 6 shows the schematic of ramp model. The shape of ramp is like half cone, and it is put directly on the flat board without diverter. Geometry parameters of cone ramp are ramp angle (θ_R) and attack angle (α) as shown in Fig.6. In the case of α = 0deg, the cone ramp is a perfect half cone with θ_R of cone angle. If α becomes larger, the shape of cone ramp comes closer to 2D wedge with θ_R of semi-apex angle.

In this study, CFD analysis was also conducted against the wedge ramp which is a basic configuration for a traditional supersonic air-inlet. As can be seen in Fig.7, the wedge ramp is also put on the flat board directly, and its geometry parameter is ramp angle (θ_R).

Table 1 shows the setting values of each geometry parameter.

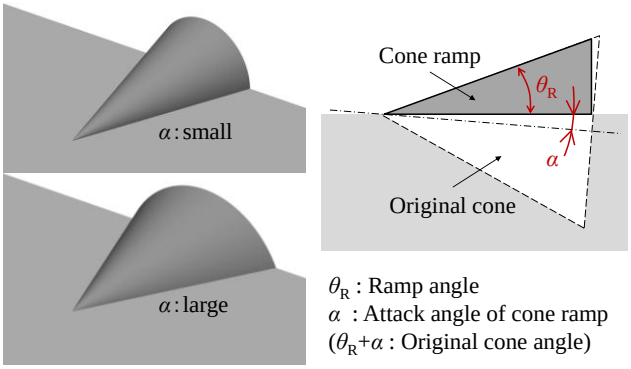

Fig.6 Cone Ramp model

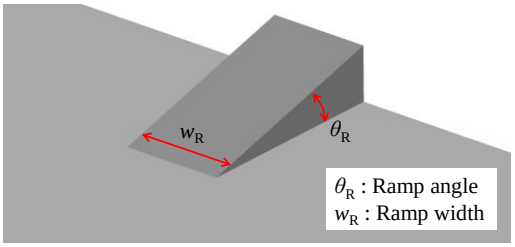

Fig.7 Wedge Ramp model

Table 1 Parameter of ramp (CFD)

	Cone	Wedge
Ramp angle θ_R〔deg〕	16, 18, 20, 22	11, 13, 15, 17
Attack angle α〔deg〕	0, 4, 8	-

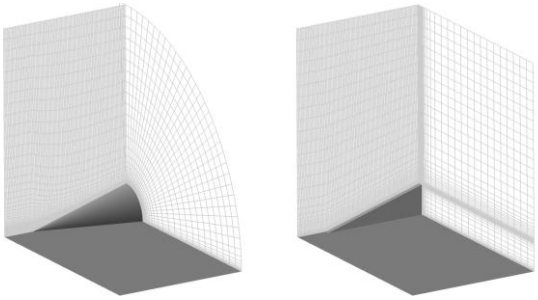

(a) Cone ramp (b) Wedge ramp

Fig.8 Computational grid for ramp flow

3.2 CFD Analysis

Flow fields around each ramp were calculated by using computational grids with 2.5 million points shown in Fig.8. The numerical calculation was conducted using the same computational code which solved the flow field around the diverter.

The numerical calculation was carried out at free stream Mach number of 1.6, which was determined by reference to the cruising speed of next generation SST suggested by JAXA [1]. The Reynolds number based on the ramp width (w_R, see Fig.7) was 5×10^5. In order to examine effects of ramp to a boundary-layer, thick boundary layer approached the ramp edge. The boundary-layer thickness ($\delta_{99\%}$) was about 0.35 times the characteristic length (w_R).

3.3 Aerodynamic Performance of Ramp

Ramps were evaluated in terms of boundary-layer thickness flows into a subsonic diffuser, and its compression performance. Because the role of ramp is compressing the air-flow which flow in subsonic diffuser, it is thought that aerodynamic performances of ramp should be evaluated at an entry face of subsonic diffuser. However, the ramp model doesn't have

subsonic diffuser. In order to achieve knowledge for ramp design which compress air-flow sufficiently and decrease boundary-layer flows to subsonic diffuser, CFD datum on the symmetry surface was used for evaluation.

The compression performance was evaluated using averaged pressure coefficient ($C_{p,ave}$) on ramp surface. In particular, pressure coefficients on symmetry line from the ramp edge to characteristic length (w_R) were averaged.

The boundary-layer thickness was evaluated using a displacement thickness at symmetry surface. However, it was thought difficult to determine main flow behind the shock-wave occurs from the ramp edge. In this study, the free stream direction velocity at $\delta_{99\%}$, $U_{99\%}$, was defined as characteristic velocity. The displacement thickness around a ramp, $\delta^*_{99\%}$, was calculated as

$$\delta^*_{99\%} = \frac{1}{U_{99\%}} \int_0^{\delta_{99\%}} U_{99\%} - u dz \qquad (1)$$

where u denotes a distribution of free stream direction velocity in the boundary-layer, and z represents the direction normal to the flat board. Furthermore, the integral interval of z direction was from a wall surface to $\delta_{99\%}$.

3.4 Results and Discussion

3.4.1 Flow Field around a Cone Ramp

In this section, the flow field around a cone ramp will be examined before discussion of the effect of the ramp configuration to the aerodynamic performance. In order to do that, the numerical calculation results of cone ramp with θ_R=18deg and α=0deg will be shown below.

Figure 9 shows the boundary-layer distribution on the symmetry surface. In the graph, the abscissa axis (x) represents the non-dimensional distance from the ramp edge.

A sharp rise of displacement thickness ($\delta^*_{99\%}$) was found at the upstream of ramp edge (x=0.0). Figure 10 (b) shows the surface pressure on the cone ramp and the flat board. There was a pressure distribution at the upstream of ramp edge. These high pressures came from behind the shock-wave through the subsonic region of boundary-layer. Thus,

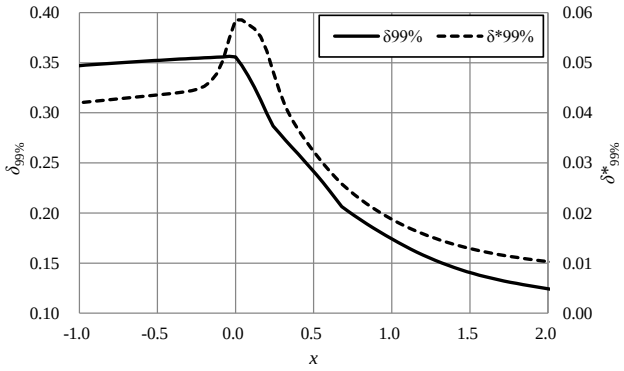

Fig.9 Boundary-layer distribution on symmetry surface (θ_R=18deg, α=0deg)

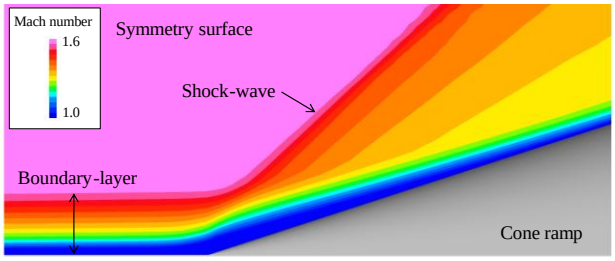

(a) Mach number distribution on symmetry surface

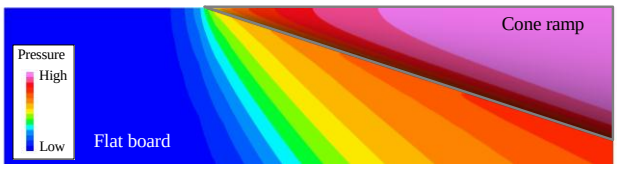

(b) Pressure distribution on ramp surface and flat board

Fig.10 Flow field around a cone ramp (θ_R=18deg, α=0deg)

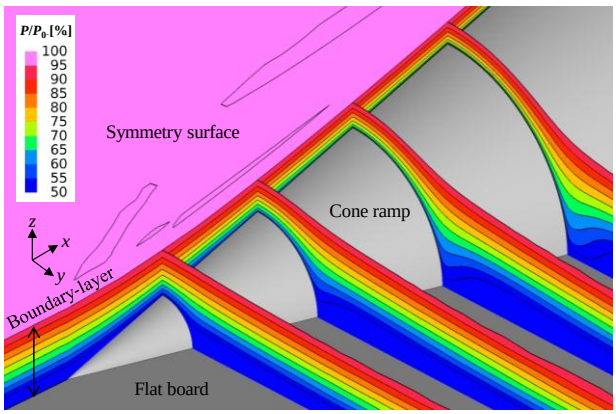

Fig.11 Total Pressure distribution around a cone ramp

increase of displacement thickness was caused by the adverse pressure gradient due to the shock-wave.

Next, the displacement thickness decreased at the downstream of ramp edge, and it became smaller than the original displacement thickness (approximately 0.045, see Fig.9). This was because that the boundary-layer thickness ($\delta_{99\%}$)

decreased with distance from the ramp edge. Figure 11 shows the total pressure distribution around a cone ramp. It can be found that the boundary-layer on the ramp surface expanded in a circumferential direction and became thinner with the distance from the ramp edge, because the cone ramp increased its cross-sectional area.

3.4.2 Effect of Cone Ramp Configuration

In order to examine the effect of cone ramp configuration to the compression performance, changes of averaged pressure coefficient ($C_{p,ave}$) are shown in Fig.12.

Regardless of attack angle (α), the cone ramp with larger ramp angle (θ_R) was better at compression performance, because the shock-wave which occurs from the ramp edge became stronger.

When θ_R was constant, the come ramp with larger α yields the better compression performance. The rate of increase in the cross-sectional area of cone ramp becomes large with the increase of α. That is to say, the shock-wave became strong in order to turn the flow largely, and the compression performance was improved.

Next, cone ramps will be evaluated in terms of boundary-layer thickness. Figure 13 shows displacement thicknesses ($\delta^*_{99\%}$) located the characteristic length (w_R) away from the ramp edge.

It is found that changes in the displacement thickness due to ramp angle (θ_R) were small. Boundary-layer distributions of cone ramps which differ in measure of θ_R are shown in Fig.14. At the ramp edge (x=0.0), the displacement thickness of θ_R=22deg was thicker

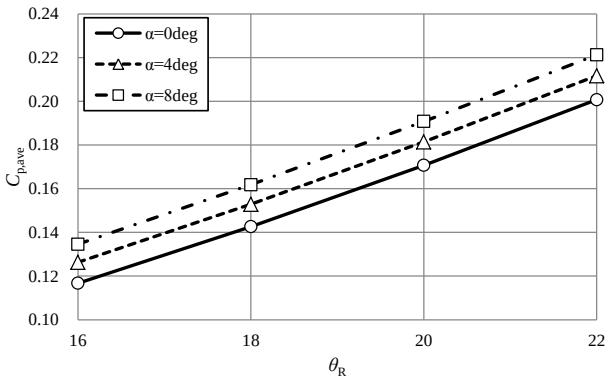

Fig.12 Compression performance of cone ramp

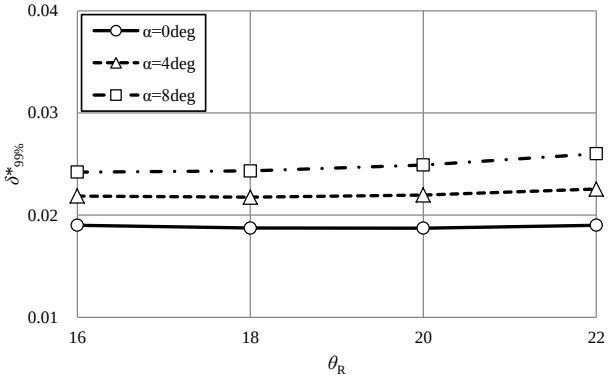

Fig.13 Displacement thickness on cone ramp

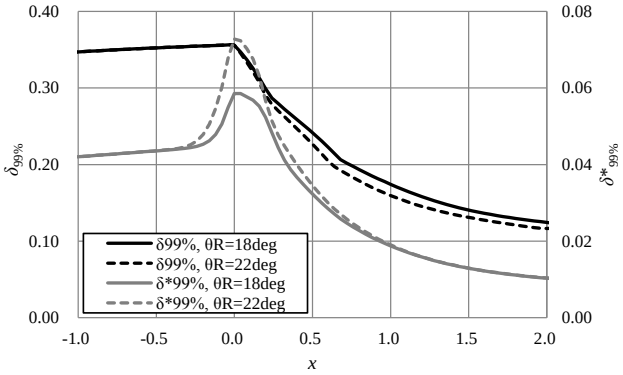

Fig.14 Boundary-layer distribution on symmetry surface (α=0deg)

than that of θ_R=18deg, because the adverse pressure gradient due to the shock-wave becomes strong with the increase of θ_R. However, at the downstream of ramp edge, the difference of displacement thickness becomes gradually small. This is because that the rate of increase in the cross-sectional area of cone ramp became large with the increase of θ_R, and the boundary-layer expanded further in a circumferential direction. As can be seen in Fig.14, the boundary-layer thickness ($\delta_{99\%}$) of θ_R=22deg was thinner than that of θ_R=18deg at downstream of ramp edge.

In Fig.13, the displacement thickness became thick with increase of α. The total flow of boundary-layer comes from ramp edge increased with increase of α, because the shape of cone ramp came close to 2D wedge as described previously. Hence, it is thought that the effect of expansion in a circumferential direction to the boundary-layer was decreased relatively, and the displacement thickness became thick.

Figure 15 shows the aerodynamic performance of cone ramps and wedge ramps

examined using CFD analysis. In the graph, the displacement thickness ($\delta^*_{99\%}$) is on the y-axis, and the averaged pressure coefficient ($C_{p,ave}$) is on the x-axis. The relationship between aerodynamic performance and ramp angle (θ_R) is represented as lines connecting data points. For example, $C_{p,ave}$ becomes large with increase of θ_R.

If the cone ramp achieves the same compression performance with the wedge ramp, for example at $C_{p,ave}$ =0.12 in Fig.15, the cone ramp makes the boundary-layer thinner than the wedge ramp. This result implies that the boundary-layer flows into a subsonic diffuser will be decreased by bringing the cone ramp to the design of supersonic air-inlet.

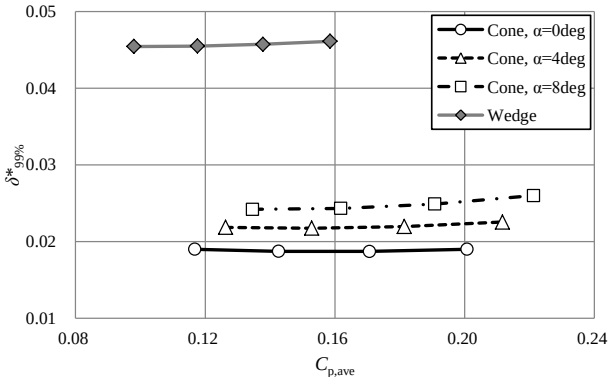

Fig.15 Performance map of ramp (CFD)

3.5 Wind Tunnel Test

The wind tunnel test was carried out at 1m×1m Supersonic Wind Tunnel owned by JAXA. The test was conducted with a wind tunnel free stream Mach number of 1.6 and Reynolds number of 2.6×10^7/m.

Figure 16 shows the wind tunnel model used in the test. The model consisted of a fuselage made of a part of Sears-Haack body [6], a ramp, a diverter, and a movable Pitot rake. As can be seen in Fig.17, pressure sensitive paint (PSP) [7] was painted on the surface of fuselage and ramp. The Pitot rake was installed at the downstream of ramp, and measured a boundary-layer.

The wedge ramp used in the test was curved around the fuselage (see Fig.17 (a)). Table 2 shows the setting values of each geometry parameter. Incidentally, the ramp length was 70mm. Furthermore, the gap between the ramp

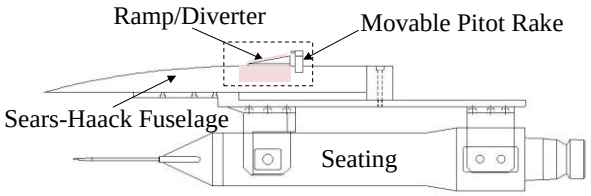

Fig.16 Wind tunnel model

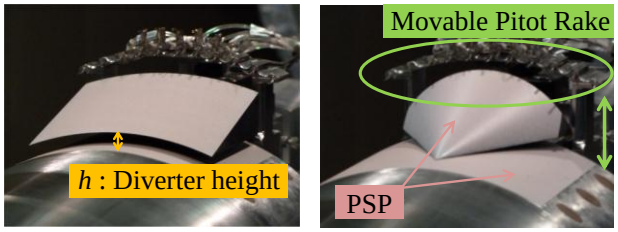

(a) Wedge ramp (b) Cone ramp
Fig.17 Ramp configuration

Table 2 Parameter of ramp and diverter (experiment)

	Cone	Wedge
Ramp width w_R [mm]	-	81
Ramp angle θ_R[deg]	18, 20	11, 14
Attack angle α[deg]	5, 10	-
Diverter height h[mm]	0	0, 3

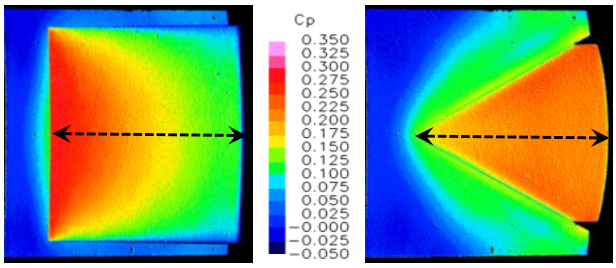

(a) wedge ramp (b) Cone ramp
Fig.18 Results of PSP measuring

edge and fuselage surface was defined as diverter height (h), and used as the geometry parameter. The boundary-layer thickness ($\delta_{99\%}$) at the ramp edge was approximately 6mm.

In wind tunnel test, the compression performance was evaluated using results of PSP measuring. Figure 18 shows examples of pressure distribution around the ramp measured by PSP. The averaged pressure coefficient ($C_{p,ave}$) was calculated from pressure datum in the middle of ramp surface (dashed line) correspond to the symmetry line of CFD analysis. Furthermore, the displacement thickness ($\delta^*_{99\%}$) on the ramp surface was calculated from measuring results of Pitot rake.

Figure 19 shows the result of aerodynamic performance evaluation in the wind tunnel test. The arrangement of graph is same to Fig.15.

When comparing the cone ramp and the wedge ramp at the same compression performance, the boundary-layer thickness on the cone ramp was thinner than that on the wedge ramp with diverter. Therefore, it was confirmed experimentally that the cone ramp is better at decreasing the thickness of boundary-layer than the wedge ramp.

The trend of compression performance due to the cone ramp configuration agrees fairly well with the CFD analysis. However, experimental results disagree with CFD results in about the boundary-layer thickness. It is thought to be a primary cause of this discrepancy that the measurement accuracy of Pitot rake was not sufficiently to measure the difference between very thin boundary-layers on each cone ramp surface.

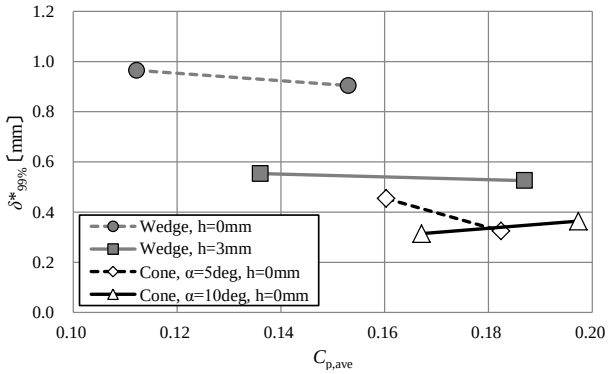

Fig.19 Performance map of ramp (experiment)

4 Conclusion

For the purpose of establishing the design guideline of diverter, indices of diverter performance were set in terms of both airframe aerodynamics and inlet performance, and the parametric study on diverter configurations was conducted using CFD simulation. It was found that the width of diverter should be set to the minimum value firstly in the design process of diverter, because the diverter performance is improved with thinning of diverter. Then, the apex angle and the height which exhibits trade-off in the diverter performance should be optimized.

Furthermore, in order to gain the knowledge for design of ramp for diverterless supersonic inlet, CFD analysis was employed to evaluate the aerodynamic performance of ramp. The wind tunnel test was also performed to validate the results of CFD analysis. It was found that the cone ramp is better at decreasing the thickness of boundary-layer than the wedge ramp. The cone ramp is one of the effective measures to reduce the boundary-layer flows into a subsonic diffuser.

References

[1] Horinouchi S. Future of the Next Generation Supersonic Airplane. *NAGARE*, Vol. 25, No. 4, pp 1-11, 2001. pp 337-344, 2006. (in Japanese)

[2] Kawai R T, Friesman D M and Serrano L. Blended Wing Body (BWB) Boundary Layer Ingestion (BLI) Inlet Configuration and System Studies. *NASA/CR-2006-214534*, 2006.

[3] Seddon J and Goldsmith E L. *Intake Aerodynamics*. 2nd edition, AIAA Education Series, 1999.

[4] Flamm J D and Wilcox F J Jr. Drag Measurements of an Axisymmetric Nacelle Mounted on a Flat Plate at Supersonic Speeds. *NASA Technical Memorandum 4660*, 1995.

[5] Fujiwara H, Watanabe Y and Sakata K. Numerical Simulation and Wind Tunnel Test of the Internal Flow through the Mach 2 Air-Intake Designed for NAL Experimental Airplane. *99 FEDSN 3rd ASME/JSME Joint Fluids Engineering Conference*, San Francisco USA, 1999.

[6] Sears W. On Projectiles of Minimum Wave Drag. *Quarterly of Applied Mathematics*, Vol. 4, No. 4, pp 361-366, 1947.

[7] Nakakita K et al. Pressure-sensitive paint test using a SST configuration model at the NAL 1m×1m supersonic wind tunnel. *JAXA Special Publication*, JAXA-SP-04-008, pp 17-21, 2005. (in Japanese)

Copyright Statement